Cartilage
2(2) 173–185

DOI: 10.1177/1947603510381096
http://cart.sagepub.com
SAGE

Acute Osteoclast Activity following Subchondral Drilling Is Promoted by Chitosan and Associated with Improved Cartilage Repair Tissue Integration

G. Chen[1], J. Sun[2,*], V. Lascau-Coman[1], A. Chevrier[1], C. Marchand[3], and Caroline D. Hoemann[1,3]

Abstract

Objective: Cartilage-bone integration is an important functional end point of cartilage repair therapy, but little is known about how to promote integration. We tested the hypothesis that chitosan-stabilized blood clot implant elicits osteoclasts to drilled cartilage defects and promotes repair and cartilage-bone integration. *Design:* Bilateral trochlear defects in 15 skeletally mature rabbit knees were microdrilled and then treated with chitosan–glycerol phosphate (GP)/blood implant with fluorescent chitosan tracer and thrombin to accelerate *in situ* solidification or with thrombin alone. Chitosan clearance, osteoclast density, and osteochondral repair were evaluated at 1, 2, and 8 weeks at the outside, edge, and through the proximal microdrill holes. *Results:* Chitosan was retained at the top of the drill holes at 1 week as extracellular particles became internalized by granulation tissue cells at 2 weeks and was completely cleared by 8 weeks. Osteoclasts burst-accumulated at microdrill hole edges at 1 week, in new woven bone at the base of the drill holes at 2 weeks, and below endochondral cartilage repair at 8 weeks. Implants elicited 2-fold more osteoclasts relative to controls ($P < 0.001$), a more complete drill hole bone repair, and improved cartilage-bone integration and histological tissue quality. Treated and control 8-week cartilage repair tissues contained 85% collagen type II. After 8 weeks of repair, subchondral osteoclast density correlated positively with bone-cartilage repair tissue integration ($P < 0.0005$). *Conclusions:* Chitosan-GP/blood implant amplified the acute influx of subchondral osteoclasts through indirect mechanisms, leading to significantly improved repair and cartilage-bone integration without inducing net bone resorption. Osteoclasts are cellular mediators of marrow-derived cartilage repair integration.

Keywords

animal model, marrow stimulation, osteoclast, osteochondral repair, chitosan

Introduction

Damaged cartilage fails to repair partly due to its avascular nature and the lack of a meaningful wound repair response. Microfracture and drilling are surgical "marrow stimulation" procedures used to treat focal articular cartilage lesions, where holes are pierced in the subchondral bone plate to induce bleeding at the base of the cartilage lesion and to generate conduits for marrow-derived stem cell migration into the defect.[1,2] However, instead of eliciting hyaline cartilage that contains high levels of collagen type II and glycosaminoglycan (GAG), the procedure elicits a mixed repair tissue predominantly composed of fibrocartilage that can be poorly integrated and reinjured by weight-bearing activities.[3-6] In 1976, Mitchell and Shepard[7] showed in a rabbit microfracture model that marrow-derived repair tissue can grow from microfracture holes without integrating with the exposed subchondral bone. Incomplete cartilage-bone integration was also reported in canine microfracture[8] and rabbit microdrill models of cartilage repair,[9] and detached

[1]Department of Chemical Engineering, Ecole Polytechnique, Montreal, Quebec, Canada
[2]BioSyntech Canada Inc., Laval, Quebec, Canada
[3]Institute of Biomedical Engineering, Ecole Polytechnique, Montreal, Quebec, Canada
*Present address: Piramal Healthcare (Canada), Laval, Quebec, Canada
Institution where the work reported was done: Ecole Polytechnique, Montreal, Quebec, Canada.

Corresponding Author:
Caroline D. Hoemann, Department of Chemical Engineering, Ecole Polytechnique, 2900 Edouard Montpetit, Montreal, QC, Canada H3C 3A7
Email: caroline.hoemann@polymtl.ca

repair tissue was correlated with a worse histological score.[9] Methods that improve cartilage-bone integration following marrow stimulation could generate a more therapeutic response, but little is known about the mechanisms that drive repair integration.

In skin wound repair, remodeling is an essential part of repair integration under mechanical load, where matrix degradation and synthesis are interlinked by cells that release metalloproteinases and others that release collagen.[10] In fracture repair, osteoclasts and osteoblasts form a remodeling unit that exerts a similar role.[11] Osteoclasts are large multinuclear cells known for their unique ability to resorb bone by forming a ruffled seal at the bone surface that permits local release of decalcifying acids, proteases, and tartrate-resistant acid phosphatase (TRAP).[12] *In vitro*, monocyte-derived macrophages will fuse to form functional osteoclasts in the presence of colony-stimulating factors and RANKL (receptor-activated NF-κB ligand), a cytokine member of the TNF-α superfamily (reviewed by Boyce and Xing[13]). In normal adult bone, osteoclast formation is suppressed by high levels of osteoprotegrin, a soluble decoy receptor that sequesters RANKL.[14] Following cortical bone fracture, many granulation tissue cells express RANKL,[15] which can help attract[16,17] and polarize monocytes to form osteoclasts on damaged bone.[18] Mechanical unloading can also promote osteoclast formation through signals that implicate apoptotic osteocytes.[19] Osteoclasts are commonly identified in histological bone sections by *in situ* TRAP enzyme activity,[12] which is lost during routine acid decalcification of cartilage-bone samples.[20] A role for osteoclasts in cartilage repair has yet to be established.

The wound repair response to subchondral bone damage generated in marrow stimulation therapy for cartilage repair can be therapeutically modified by application of a chitosan-stabilized blood clot implant over drilled or microfractured defects.[9,21-23] Chitosan is a biodegradable and adhesive polysaccharide scaffold of glucosamine and N-acetyl-glucosamine that, due to its unique positive charge state, can stabilize the blood clot in the cartilage lesion.[21,24] Drilled defects further treated with chitosan–glycerol phosphate (GP)/blood implant develop a more hyaline and integrated cartilage repair.[9,24-28] Chitosan clot implants also stimulate a remarkable level of trabecular bone remodeling,[24] suggesting that hybrid clot implants may promote osteoclast formation.

In the present study, we used a skeletally mature rabbit model to test the hypothesis that subchondral drilling elicits osteoclasts and that chitosan-stabilized blood clot implants elicit more osteoclasts and better cartilage-bone integration compared to drilling alone. Our histoprocessing methods were geared to preserve TRAP activity and to permit immunostaining of collagen type I and II. We also incorporated a fluorescent rhodamine B isothiocyanate (RITC)–chitosan tracer in the implants to visualize scaffold-cell interactions in repair tissues at 1, 2, and 8 weeks postoperatively in sections obtained from outside, the edge, and through the microdrill holes. This approach enabled us to clarify both the role of the microdrill holes and the role of chitosan scaffold in the formation of osteoclasts and the development of an integrated cartilage repair tissue.

Materials and Methods

Fluorescent Chitosan-GP/Blood Implants

Sterile solutions of 2% w/v chitosan-HCl (80% degree of deacetylation [DDA], Mn = 179 kDa, polydispersity index [PDI] = 1.4, <500 EU/g, <0.2% protein/g, pH 5.6) and 500 mM disodium β-glycerol phosphate/50 mM HCl (pH 7.2) (GP) were provided by BioSyntech Inc. (Laval, Quebec, Canada). RITC-chitosan with 80% DDA, Mn = 145 kDa, PDI = 1.3, and 0.5% mol/mol RITC/chitosan[29] was dissolved at 5 mg/mL in 23 mM HCl, filter-sterilized, and stored at –80 °C. Prior to surgery, chitosan-HCl (0.4 mL) was combined aseptically with RITC-chitosan (0.1 mL) and GP (0.1 mL) in flat-bottomed 2.0-cc cryovials (Corning, Fisher Scientific, Montreal, Quebec, Canada), with three 0.39-g sterile surgical steel mixing beads (Salem Specialty Ball, Canton, CT, USA) and homogeneously mixed with 1.5 mL fresh nonactivated autologous whole blood aseptically drawn from the central ear artery by vigorous manual shaking for 10 seconds.

Rabbit Surgical Model of Bone Marrow Stimulation

All animal protocols were approved by an institutional review board and carried out according to Helsinki guidelines for animal research. Sixteen skeletally mature New Zealand White rabbits (8 male, 8 female; 10-24 months old; 4.1 ± 0.5 kg) were randomly distributed in 3 groups of 1-, 2-, or 8-week repair periods. One day prior to surgery, rabbits were administered a half-dose fentanyl patch analgesic on the right ear (Duragesic 25, fentanyl transdermal system, Janssen-Ortho, CDMV, Toronto, Ontario, Canada). Rabbits were anesthetized with ketamine/xylazine/buprenorphine; then, the ears (phlebotomy site) and legs were shaved and disinfected, and under 3% isoflurane/0.8% oxygen, the trochlear knee cartilage was accessed by sequential small bilateral knee arthrotomies and parapatellar luxation. Flat surgical blades of 1.5 and 2.75 mm (Fine Science Tools, North Vancouver, British Columbia, Canada) were used to create 3.5 × 4.5-mm full-thickness articular cartilage defects debrided into the calcified layer.[9,24] Open joint surfaces were kept moist with sterile Ringer's lactated solution (RLS, Dufort Lavigne, Montreal, Quebec, Canada). Four 0.9-mm-diameter microdrill holes were created in each of

Table 1. Experiment Design of the Rabbit Cartilage Repair Study

Rabbit Groups	No. of Animals	Treated Defects Total (Left Knee, Right Knee)	Control Defects Total (Left Knee, Right Knee)
1-week repair	*N* = 4 (2 F, 2 M)	*N* = 5 (*n* = 3, *n* = 2)[a,b]	*N* = 3 (*n* = 1, *n* = 2)
2-week repair	*N* = 4 (2 F, 2 M)	*N* = 5 (*n* = 3, *n* = 2)[a,b]	*N* = 3 (*n* = 1, *n* = 2)[c]
8-week repair	*N* = 7 (2 F, 5 M)	*N* = 7 (*n* = 3, *n* = 4)	*N* = 7 (*n* = 4, *n* = 3)

Note: F = female; M = male.
[a]One rabbit in the 1-week group and one rabbit in the 2-week group had bilateral treated defects (± thrombin).
[b]Two defects in this group were embedded in methyl methacrylate (MMA).
[c]One defect in this group was embedded in MMA.

the 4 corners of the defect using a high-speed, hand-held microdrill (Fine Science Tools) with constant irrigation with RLS to prevent thermal necrosis and wash away bone debris. A pilot study was performed in 2 rabbits to verify that the use of thrombin (to accelerate *in situ* solidification of chitosan-GP/blood[30]) gave a similar repair response as implant without thrombin. These 2 rabbits were treated bilaterally with RITC-chitosan-GP/blood implant with and without preapplication on the defect of 3 µL of 45 or 50 U/mL purified human thrombin (tissue-culture grade, Sigma-Aldrich, Oakville, Ontario, Canada) (**Table 1**). In an additional 14 rabbits, alternating left and right drilled defects were treated by applying 3 µL of 45 or 50 U/mL thrombin followed within 10 to 60 seconds by 1 hanging drop (~25 µL) of RITC-chitosan-GP/blood mixture, while the contralateral defect was treated with 3 µL of thrombin alone. Since thrombin was a controlled variable, differences in the repair response could be attributed to the chitosan implant. Thrombin implants solidified with an average delay of 3.0 ± 0.9 minutes following application (*N* = 15). Knees were closed in sutured layers using prolene nonresorbable sutures (Dufort Lavigne). Animals were allowed immediate unrestrained postoperative activity in cages and received a new half fentanyl patch 3 days postarthrotomy to provide 6 days of continuous analgesia. Several treated and control knees experienced a transient effusion from 1 to 2 weeks postoperatively, with no signs of infection of any knees at necropsy. The heaviest 24-month-old male rabbit in the study (5.60 kg) experienced an unscheduled death at 3 days postoperatively due to apparent complications from surgical anesthesia. Therefore, at 1, 2, or 8 weeks postoperatively (**Table 1**), 30 defects were collected from 15 rabbits following euthanasia by sodium pentobarbital intravenous injection under anesthesia. Intact femurs were collected from 4-month-old (4 femurs from 3 rabbits) and 12-month-old (4 femurs from 2 rabbits) rabbits as additional controls.

Macroscopic Assessments and Histoprocessing

Macroscopic retention of fluorescent implant was documented in the dissected femurs with an inverted Zeiss axiovert fluorescence microscope (EC Plan-Neofluar 1.25x/0.3 NA objective, Carl-Zeiss Canada, Toronto, Ontario, Canada), CCD Hitachi camera (Tokyo, Japan), and Northern Eclipse software (Empix, Mississauga, Ontario, Canada). Femur ends were fixed in 80% ethanol at 4 °C and either embedded nondecalcified in methyl methacrylate (MMA) plastic resin (5 defects, 5 intact femurs) or transferred to 4% paraformaldehyde/100 mM sodium cacodylate (pH 7.2) at 4 ºC (25 defects, 3 intact) (**Table 1**) and decalcified in 10% ethylene diaminetetra-acetic acid (EDTA)/0.1% paraformaldehyde at 4 ºC up to 4 months. Decalcified defects were trimmed transversely in half, the proximal half was equilibrated in sucrose and OCT, and transverse cryosections were collected using the CryoJane tape system (Instrumedics, Richmond, IL, USA). Approximately 40 sections per level (2-µm-thick MMA or 10-µm-thick cryosections) were collected from the proximal half of all defects at 3 different levels: between the microdrill holes (level 1), at the edge of the microdrill holes (level 2), and through the middle of the proximal drill holes (level 3). Transverse sections were also collected from intact trochlea.

Histostaining, Immunohistochemistry, and Enzymatic Staining for TRAP+ Osteoclasts

All materials were from Sigma-Aldrich unless otherwise indicated. MMA sections and cryosections from all 3 levels were stained with Safranin O/fast green/iron hematoxylin, immunostained for collagen type I and collagen type II, and enzymatically stained for TRAP. Immunostaining was performed as previously described.[31] Briefly, decalcified cryosections were thawed 5 minutes at room temperature followed by 5 minutes in acetone, and nondecalcified MMA sections were deplastified by 3 × 5 minutes' incubation in acetone. Sections were submitted to antigen retrieval by incubating at 60 ºC in 10 mM Tris (pH 10), followed by pronase (1 mg/mL, 30 minutes at room temperature), hyaluronidase (25 mg/mL, 30 minutes at 37 ºC), blocked with 20% normal goat serum (NGS) in phosphate-buffered saline (PBS), 0.1% TX-100, followed by monoclonal

anticollagen type I (10 µg/mL, clone I-8H5, MP Biomedical, VWR, Montreal, Quebec, Canada) or monoclonal anticollagen type II (hybridoma culture supernatant, diluted 1:10, clone II-II6B3, Developmental Hybridoma Studies Bank, Iowa City, IA, USA) in 10% NGS/PBS/0.2% TX-100, then biotinylated goat antimouse IgG (11 µg/mL, Vector, Burlingame, CA, USA), and streptavidin-biotin-alkaline phosphatase (ABC-AP) with red substrate kit containing levimasole to block endogenous alkaline phosphatase (Vector), and counterstained with Weigert iron hematoxylin. For TRAP enzymatic staining, cryosections were thawed, while MMA sections were deplastified; then, sections were pretreated for 1 hour at room temperature with 1% w/v $MgCl_2$ to restore divalent cations removed by EDTA that are essential to phosphatase activity,[32,33] preequilibrated for 20 minutes in 40 mM tartrate in 50 mM sodium acetate (pH 5.0), then incubated for 1 hour at 37 °C in staining solution (2.5 mg/mL naphathol-AS-MX predissolved in dimethyl formamide, 0.5 mg/mL diazotized Fast Garnet GBC, 40 mM tartrate in 50 mM sodium acetate, pH 5.0[33]), counterstained with methyl green (Vector), and coverslipped with aqueous mounting media.

Osteoclast Density, Quantitative Histomorphometry, and Histological Scoring

Quantitative blinded histomorphometry and TRAP+ cell density measurements were performed by one observer (G.C.) using Northern Eclipse histomorphometric software (Empix) in sections from outside the holes, hole edge, and through the drill holes (levels 1, 2, and 3). Osteoclast density per millimeter squared (mm^2) was determined by manual point counting of TRAP+ cells with osteoclast morphology adhering to trabecular bone in a region encompassing the entire subchondral defect zone (4.3 mm wide and 8-10 mm deep, excluding lateral trochlear ridges and osteophytes, if present), divided by the cross-sectional area (approximately 40 mm^2). Histomorphometry with Safranin O–stained sections carrying blinded identification numbers was carried using a line tool,[9] using the flanking cartilage to establish a slightly curved projected tidemark through the repaired defect to obtain total defect width. Line measurements were made along the projected tidemark to obtain percentage of tissues covering the defect (exposed bone, repair tissue integrated with bone, and repair tissue covering the subchondral bone but clearly detached from bone). Soft repair tissue cross-sectional area above the projected tidemark, and separately below the tidemark, was determined by volume measurements from low-magnification (1.25x) Safranin O–stained images, and percentage of Safranin O+ repair tissue was obtained by threshold analysis. Percentage of collagen type I and collagen type II repair tissue was obtained from digitally scanned images by automated threshold analysis of strong red immunostained repair tissue above the projected tidemark using Image J (RSB-NIH, Bethesda, MD) and Matlab (Mathworks, Natik, MA) to extract the hue-saturation-value (HSV) color space within threshold limits kept constant for all samples. O'Driscoll histological scoring[34] with the modification of adding another 3-point value for subchondral bone health (0 = cyst or fibrous tissue, 1 = callus, 2 = remodeling bone, 3 = normal subchondral bone) was performed by 2 independent blinded observers (G.C. and A.C.) on sections between, at the edge, and through the drill holes, and the median score (minimum-maximum) was reported.

Statistical Methods

The general linear model (GLM, Statistica version 6.1, StatSoft, Tulsa, OK, USA) was used to test the effect of treatment, time, and histological section level in the drill hole (outside, edge, and through the holes) on osteoclast density, percentage of detached repair tissue, cartilage repair volume (N = 3-5 for weeks 1 and 2, N = 7 for week 8), with LSD *post hoc* analysis to analyze univariate effects. The paired Student t test was used to evaluate the effect of treatment on percentage of Safranin O–stained repair at 8 weeks. Covariate scatterplots and multivariate correlation (Statistica, StatSoft) were used to obtain correlation coefficients between osteoclast density and percentage of integrated repair tissue at 8 weeks (3 different sections from 14 defects). Significance was set at $P < 0.05$. The Mann-Whitney U nonparametric test (Statistica, StatSoft) was used to evaluate the effect of treatment on O'Driscoll histological scores. Differences were considered significant when the blinded analysis of 2 different observers independently generated exact values of $P < 0.05$.

Results

Chitosan Particles Reside for 2 Weeks at the Top of the Microdrill Holes and Are Cleared by 8 Weeks

Implant residency was analyzed in rabbits that were immediately mobile following surgery and had unrestrained activity for the entire repair period. Fluorescent chitosan implant was macroscopically retained over all microdrill holes at 1 week postoperatively, with diminished intensity after 2 weeks, and was completely cleared after 8 weeks of repair (**Fig. 1**). These data were consistent with a previous report that fast green–stained chitosan particles were cleared by 5 weeks of repair in a similar cartilage repair model using implants without thrombin.[24] To verify the influence of thrombin on implant retention, 2 rabbits in this study received implant without and with thrombin to accelerate *in situ* solidification.[30] More RITC-chitosan was retained in defects pretreated with thrombin (**Fig. 1 C** and **D**). All other defects received either thrombin implant (treated) or

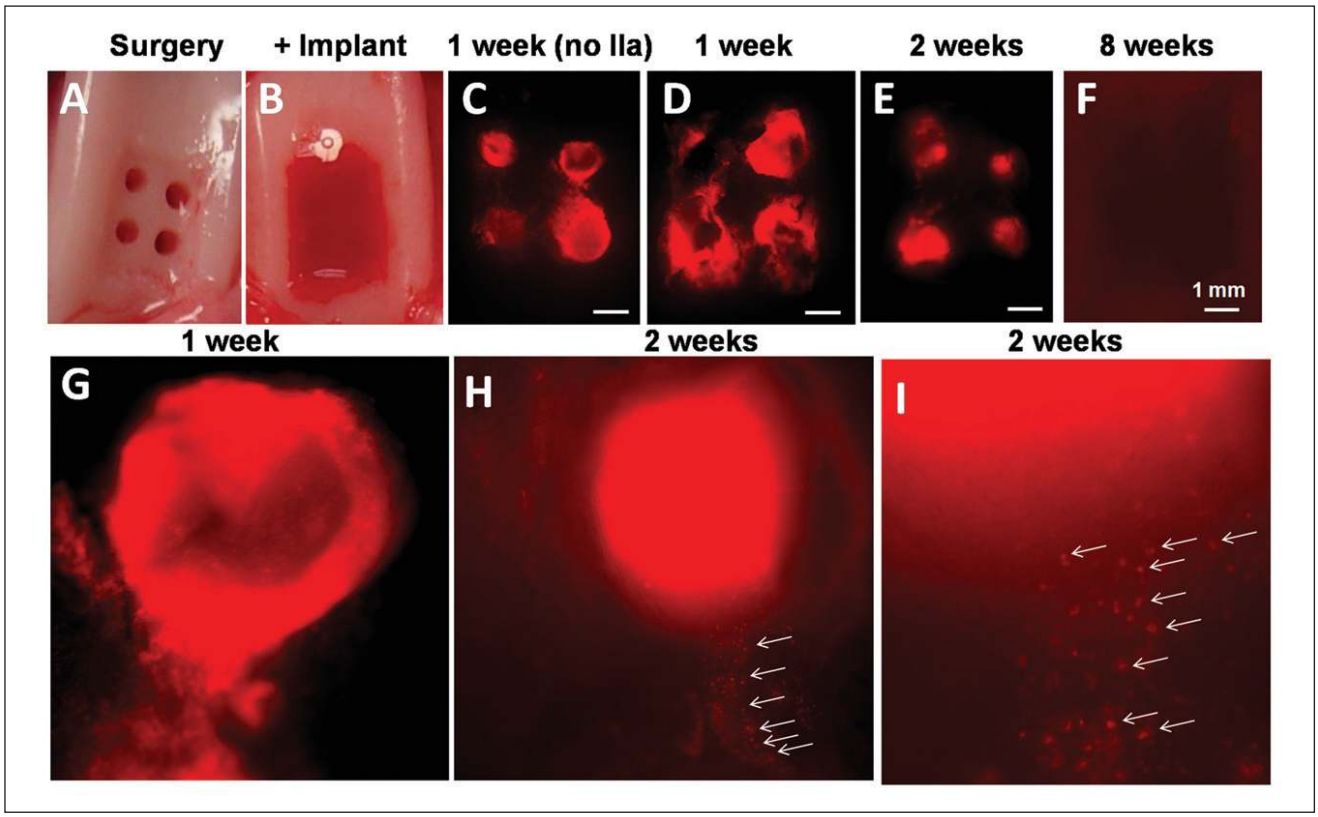

Figure 1. Residency and clearance of chitosan particles in microdrilled cartilage defects. Full-thickness cartilage defects were microdrilled (**A**) and loaded with fluorescent chitosan-GP/blood implant that solidified *in situ* (**B**). Fluorescent chitosan particles were retained over all 4 microdrill holes after 1 week *in vivo* (**C** and **D**), showed diminished fluorescent signal at 2 weeks (**E**), and were no longer detectable at 8 weeks (**F**). Implants solidified *in situ* with thrombin (**D**) retained more chitosan than implants solidified without thrombin (**C**) (representative data from $N = 2$). Extracellular chitosan at 1 week (**G**) was internalized by repair cells at 2 weeks (**H** and **I**, white arrows). Scale bars in panels **C** to **F** are 1 mm.

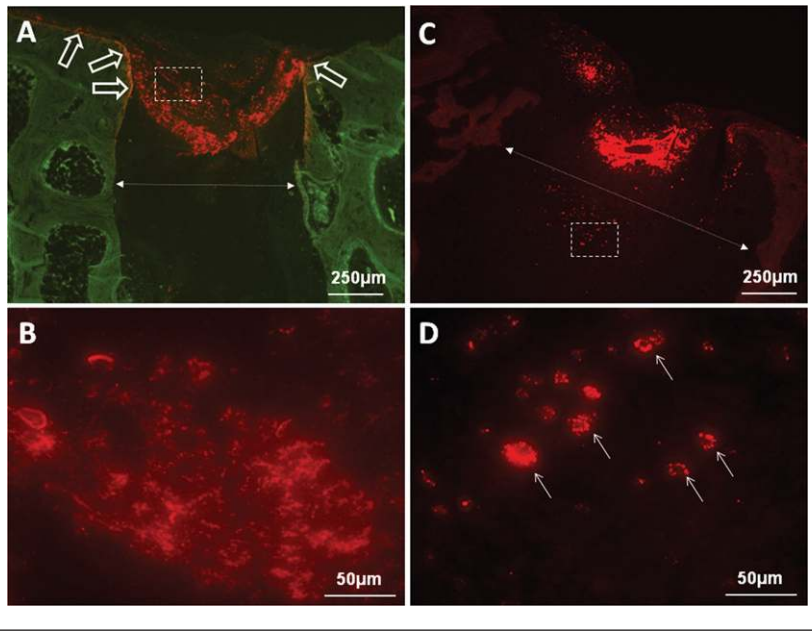

Figure 2. Dynamic distribution of chitosan particles during articular cartilage regeneration in microdrilled cartilage defects, in unstained plastic sections. The red fluorescent signal shows RITC-chitosan, and the green (**A**) is autofluorescent bone. After 1 week of repair, chitosan particles resided at the top of drill holes (**A**) as an extracellular scaffold dispersed within the fibrin clot (**B**). Some chitosan adhered to the bone lining the drill hole side walls and the base of the defect (**A**, open arrows). At 2 weeks of repair, little or no extracellular chitosan remained (**C**), and most chitosan particles were internalized in vesicles of granulation tissue cells (**D**). The dotted arrows (in **A** and **C**) show the increased width of the treated drill hole at 2 weeks.

thrombin only (control). Since thrombin was a controlled variable, repair reactions in treated defects could be attributed to the chitosan clot implant.

In histological sections, fluorescent chitosan particles were limited to the top of the drill holes (**Fig. 2 A** and **C**). Particles became transformed from an extracellular scaffold at 1 week to intracellular vesicles in granulation tissue cells at 2 weeks (**Fig. 1 G-I** and **Fig. 2 B** and **D**). Occasional fluorescent implant fragments were seen in the fat pad or synovium lining the trochlear ridge (data not shown). At 1 week, some chitosan coated the bone surfaces at the top of the drill hole and along the base of the defect (**Fig. 2A**, open arrows). To summarize, these data showed that chitosan particles resided at the top of all treated drill holes and were actively cleared over several weeks by granulation tissue cells.

Osteoclast Activity Is Promoted by Chitosan-GP/Blood Implant through Indirect Mechanisms

Osteoclasts accumulated below drilled cartilage defects in 3 distinct phases: resorption, remodeling, and endochondral cartilage repair formation. At 1 week postoperatively, osteoclasts accumulated along the edges of the drill holes (**Fig. 3 A-B**), and in some treated defects, osteoclasts appeared to be tunneling toward the chondral defect surface (**Fig. 3C**). After 2 weeks, osteoclasts appeared in remodeling new woven bone at the base of the repairing drill holes, with osteoblasts in the vicinity (**Fig. 3 D-F**). At 8 weeks, osteoclasts were detected in vascularized bone pores in the subchondral bone plate below integrated endochondral repair tissue (**Fig. 3 G-J**). Except for the top of the drill holes, osteoclasts below treated defects at 1 to 2 weeks did not appear to be in direct contact with RITC-chitosan particles (compare **Fig. 2C** with **Fig. 3E**). Higher osteoclast density below treated defects at 8 weeks was not directly due to the chitosan implant, which was completely cleared at this time point (**Fig. 1F**). Although apoptotic osteocytes can mediate osteoclast formation in some contexts,[19] at 1 week after drilling, we found no clear evidence of osteocyte apoptosis at the drill hole edges lined with osteoclasts (**Fig. 4A**). Small mononuclear TRAP+ cells with spindle-shaped (nonosteoclast) morphology were detected in some drill hole granulation tissues in both control and treated defects (**Fig. 4B**, open arrow); these cells were excluded from osteoclast density measurements.

The net effect of implant was to double the osteoclast density lining the drill holes at 1 week ($P < 0.0001$) (**Fig. 5A**). The chitosan implant also expanded the zone of acute osteoclast formation to subchondral areas between the drill holes at 1 week (**Fig. 5A**, level 1). After 2 weeks, osteoclast density increased below control defects, mainly along new woven bone forming at the base of all drill holes, and was slightly higher below treated defects ($P = 0.023$) (**Fig. 5B**, level 2). At 8 weeks, osteoclast density subsided, with more osteoclasts detected below treated than control defects ($P = 0.023$) (**Fig. 5C**). Osteoclast density in 8-week repair bone was similar to that of intact immature 4-month-old rabbit trochlea (**Fig. 5C**, horizontal arrow, 8 weeks). Osteoclasts were scarcely detected in sections from adult rabbits (**Fig. 5C**, horizontal circle arrow, 8 weeks).

Implants Improve Cartilage Repair Integration, Structural Integrity, and Histological Quality

Drill holes were mainly filled with a hypocellular fibrin clot at 1 week and with granulation tissues at 2 weeks as previously observed in microdrilled rabbit defects.[24] At 1 week, more tissue was retained above the projected tidemark in treated than control defects ($P = 0.012$) (**Fig. 5D**), indicating that chitosan had stabilized the blood clot in the cartilage defect. At 2 weeks, however, only a very thin layer of granulation tissue remained above the projected tidemark (**Fig. 5E**). After 8 weeks of repair, more repair tissue was present in the control defects compared to treated ($P < 0.001$) (**Fig. 5F**), even more than that normally present in a similar-sized area from intact rabbit trochlea (**Fig. 5F**, horizontal arrows).

In 2-week control repair tissues, we observed that marrow-derived tissue tended to form more cohesive bonds within the newly formed repair matrix rather than attaching to the bone (**Fig. 6A2**). This morphology was frequently followed at 8 weeks by repair tissue "sprouting" from the drill holes without attaching to the bone base of the defect (**Fig. 6B**). Treated repair tissues formed cell-bone matrix attachments at 2 weeks (**Fig. 6C**), which was followed by integrated repair at 8 weeks (**Fig. 6D**). In quantifying the percentage of repair tissue detached from the bone base of the defects, we noted that fibrin clot and granulation repair tissues were quite fragile and could tear during cryosectioning; however, detached repair tissues observed at 8 weeks showed smooth repair tissue surfaces facing the bone, suggesting the tissue was detached *in vivo* and not a sectioning artefact (**Fig. 6B2**). After 1 to 2 weeks of repair, all defects showed a similar level of tissue detachment (**Fig. 5 G** and **H**), but after 8 weeks of repair, control defects showed significantly more detached cartilage repair throughout the proximal defect ($P < 0.001$) (**Fig. 5I**), especially at the edge of the drill hole (**Fig. 5I**, level 2, 8 weeks). Control tissues tended to be depleted of glycosaminoglycan at the edge of the hole ($P = 0.066$) (**Fig. 5J**, level 2).

Treated repair tissues over the drill holes had consistently more chondrocyte-like cells (O'Driscoll histological scores I and VII) (**Table 2**), higher structural integrity, healthier subchondral bone, and a higher total histological score

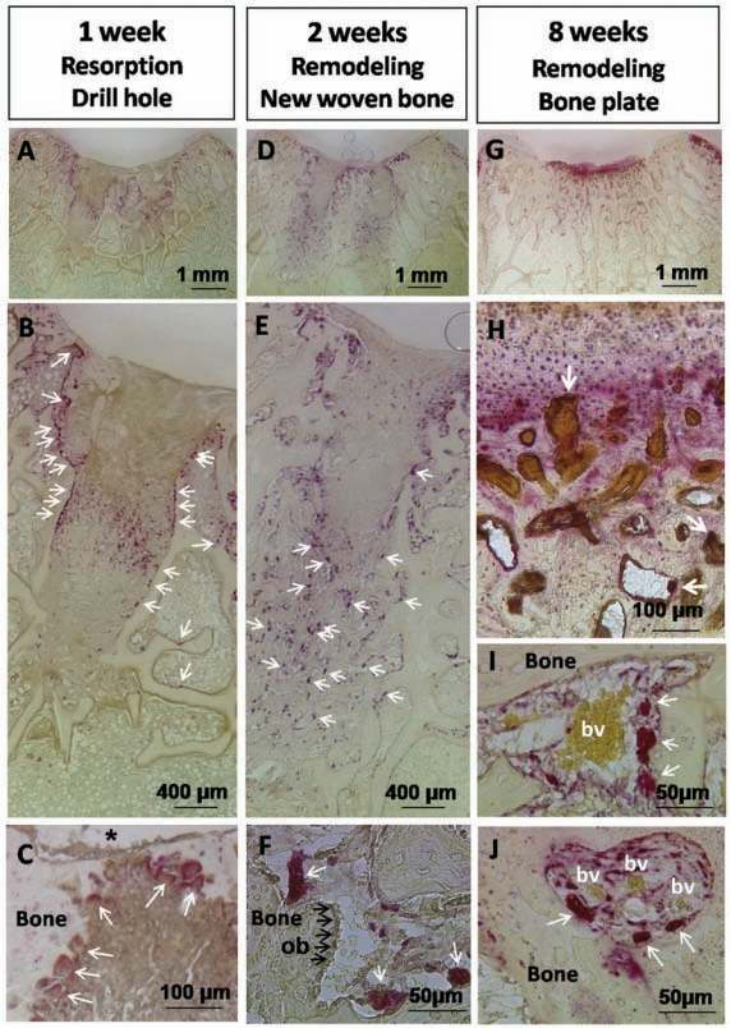

Figure 3. Osteoclasts followed 3 phases of recruitment to repairing drilled osteochondral defects after 1 week (**A-C**), 2 weeks (**D-F**), and 8 weeks of repair (**G-J**). Sections were stained enzymatically for TRAP+ osteoclasts (red-brown stain, white arrows). The asterisk indicates the defect surface (**C**), the black arrows indicate osteoblasts (ob) (**F**), and "bv" indicates blood vessels (**I** and **J**).

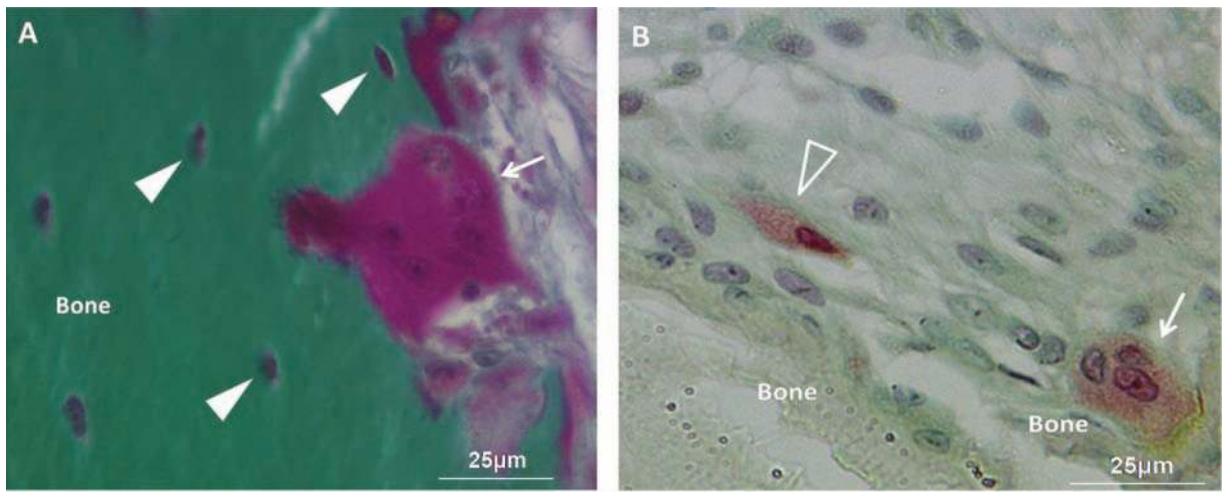

Figure 4. Osteoclast morphology in nondecalcified plastic sections from repairing defects. (**A**) An example of multinucleated osteoclast (white arrow) adhering to bone lining the drill hole adjacent to viable osteocytes (white arrowheads, Goldner-stained section from 1-week repair, treated defect). (**B**) An osteoclast (white arrow) and a typical mononuclear TRAP+ cell detected in granulation tissue with nonosteoclast morphology (open arrowhead, TRAP-stained section with methyl green counterstain from 2-week repair).

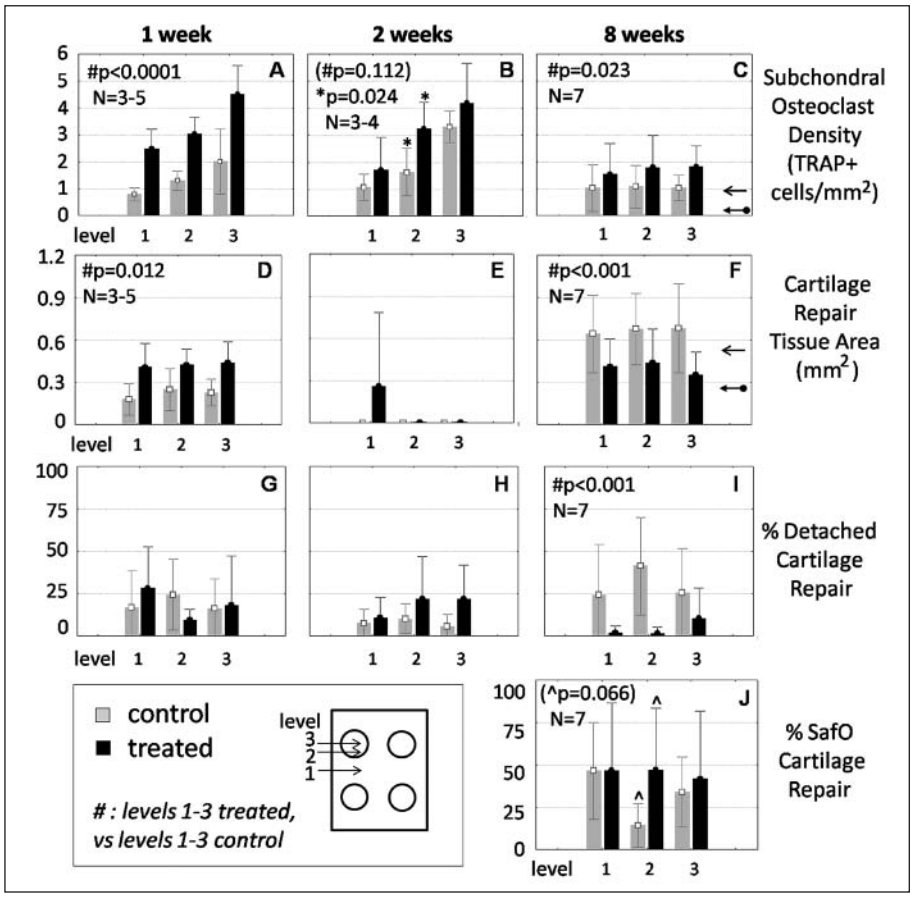

Figure 5. Treatment with thrombin-chitosan-GP/blood implant versus thrombin alone resulted in time-dependent alterations in subchondral osteoclast density (**A**), soft repair tissue formation (**B**), and repair integration (**C**) at 1, 2, and 8 weeks postoperatively and led to similar Safranin O–stained matrix at 8 weeks postoperatively (**D**), according to quantitative histomorphometry. Data show the average ± 95% confidence intervals. Levels 1, 2, and 3 refer to sections analyzed between, at the edge, and through the drill holes as indicated by the schematic. Significant differences specifically due to treatment (#) were analyzed at each time point using the general linear model (GLM), where all 3 levels were simultaneously analyzed with treatment as a predictor. *Significant effect due to treatment level 2 only (GLM with LSD *post hoc*). ^Nearly significant effect due to treatment for level 2 (paired Student *t* test). The arrow and circle arrow (**C** and **F**, right panels) show average values obtained from intact knee trochlea of immature ($N = 4$) and skeletally mature ($N = 4$) rabbit femurs, respectively.

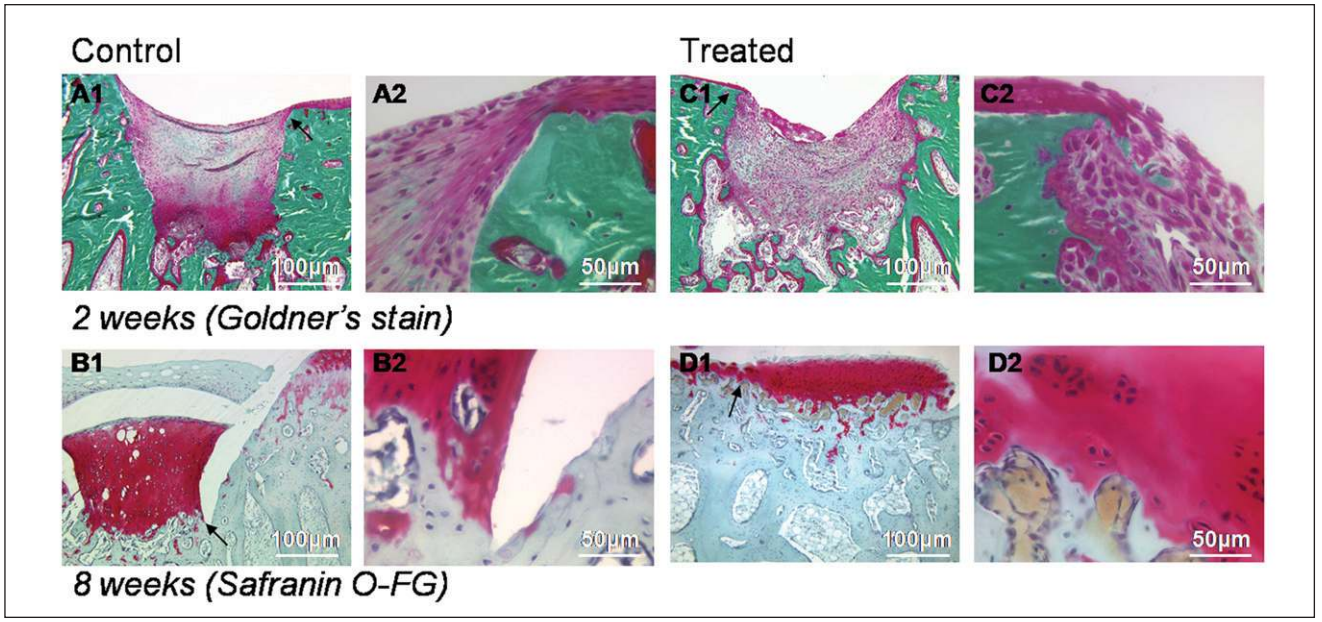

Figure 6. An example of integration of repair tissues at 2 weeks (top panels, nondecalcified plastic sections) and 8 weeks (bottom panels, decalcified cryosections) in control (**A** and **B**) and treated (**C** and **D**) defects. The black arrows in **A1**, **B1**, **C1**, and **D1** indicate the region shown in the adjacent panel.

Table 2. Histological O'Driscoll Scores, Median (Range), of 8-Week Repaired Trochlear Defect Sections (n = 7)

	Between Drill Holes		Over Drill Holes	
	Untreated	Treated	Untreated	Treated
I. Chondrocyte cell morphology (0-4)	2 (1-3)	3 (0-4)	2 (1-3)*	3 (1-4)*
II. Safranin O stain (0-3)	2 (0-3)	1 (0-3)	1 (1-2)	2 (1-3)
III. Surface regularity (0-3)	1 (1-3)	2 (0-3)	1 (0-2)	2 (1-3)
IV. Structural Integrity (0-2)	1 (0-2)	2 (0-2)	0 (0-2)**	2 (1-2)**
V. Thickness (0-2)	1 (1-2)	1 (0-2)	1 (0-2)	1 (0-2)
VI. Bonding with adjacent cartilage (0-2)	0 (0-1)	0 (0-1)	0 (0-2)	0 (0-1)
VII. Normal cellularity (0-3)	2 (0-3)	3 (0-3)	3 (0-3)	3 (0-3)
VIII. No chondrocyte clustering (0-2)	1 (1-2)	1 (0-2)	1 (1-2)	1 (1-2)
IX. Free from degeneration in adjacent cartilage	3 (1-3)	2 (1-3)	2 (1-3)	1 (1-2)
X. Subchondral bone health (0-3)	1 (0-3)	2 (0-3)	0 (0-1)***	2 (1-2)***
Total score (maximum: 27)	14 (8-18)	18 (6-20)	13 (8-16)****	18 (13-22)****

*P = 0.026. **P = 0.011. ***P = 0.0011. ****P = 0.0023.

(scores IV, X, and total) (**Table 2**). Significant histological differences due to treatment were only observed in sections through the drill holes in this relatively small sample group (N = 7). Most repair tissues were not bonded with adjacent cartilage, and all adjacent cartilage tissues showed some degree of degeneration. Collagen typing of the repair tissues at 8 weeks showed that treated and control repair matrix contained the same average area percentage of collagen type II (85%) and collagen type I (38%) (**Fig. 8A**). This result was partly due to a poor cartilage repair response in 2 of the 7 treated rabbits in the 8-week group that were skeletally aged to 24 months see (**Fig. 7 O** and **P**). Treated drill holes were slightly larger at 1 to 2 weeks than controls (**Fig. 8 B** and **C**) and more completely repaired with bone at 8 weeks compared to controls (**Fig. 8D**), which were frequently filled with collagen type II instead of collagen type I matrix (**Fig. 7 C** and **D**).

Osteoclast Density Correlates with Endochondral Repair Integration

At 8 weeks of repair, most repair cartilage with hyaline features was integrated with a cartilage-bone interface carrying the "tell-tale signs" of endochondral ossification, including patches of GAG in a porous and vascularized subchondral bone plate (**Fig. 6D**). Osteoclasts were mainly detected in the subchondral bone plate below integrated hyaline repair (**Figs. 3 H-J** and **7F**). Multiple correlation analysis revealed a highly significant relationship between TRAP+ subchondral osteoclast density and histomorphometric line measurements of percentage of integrated repair (R = 0.54, P = 0.00027) (**Fig. 9**). These data showed that after 8 weeks of repair, osteoclasts were attracted to areas of integrated endochondral repair through chitosan-independent mechanisms.

Discussion

Osteoclasts Are Recruited to Drilled Subchondral Bone

While osteoclast activity has been reported in cortical bone fracture repair,[12,18] inflammatory arthritis,[35] bone remodeling,[13] and growth plate ossification,[36] little is known of osteoclast activity in trabecular bone during cartilage repair. To the best of our knowledge, this study is the first to report that osteoclasts are elicited by a cartilage repair procedure that involves subchondral bone damage. Drilling under irrigation with RLS removes bone-lining cells from trabeculae and creates microdamage at the bone surface, without however inducing acute osteocyte necrosis in bone lining the drill holes.[37] *In situ* solidification of chitosan-GP/blood implant over the drill holes enhanced initial resorption of the drill holes (**Fig. 2C**) through mechanisms that were not explained by local osteocyte apoptosis (**Fig. 4A**). Enhanced acute osteoclast activity was followed by the formation of a more mechanically integrated endochondral unit (**Fig. 6D**). These data suggest that bone repair cartilage integration is aided by "wound bloom," a critical step in which a marginal increase in bone lesion size promotes anatomical incorporation of regenerated tissue.

There are several mechanisms that could explain enhanced osteoclast recruitment to chitosan-treated drill holes. Biodegradable chitosan is chemotactic for neutrophils[24,26,38,39] and macrophages,[27,39] and since osteoclasts are derived from monocytes that extravasate to bone, bulk attraction of macrophages to extracellular chitosan particles could partly explain the increased osteoclast density below treated defects during the inflammatory repair phase at 1 week. Chitosan could potentially induce neutrophils[40] or granulation tissue cells[15] to release RANKL. Future studies will show whether osteocytes below the chitosan implant release osteoclast-promoting factors.

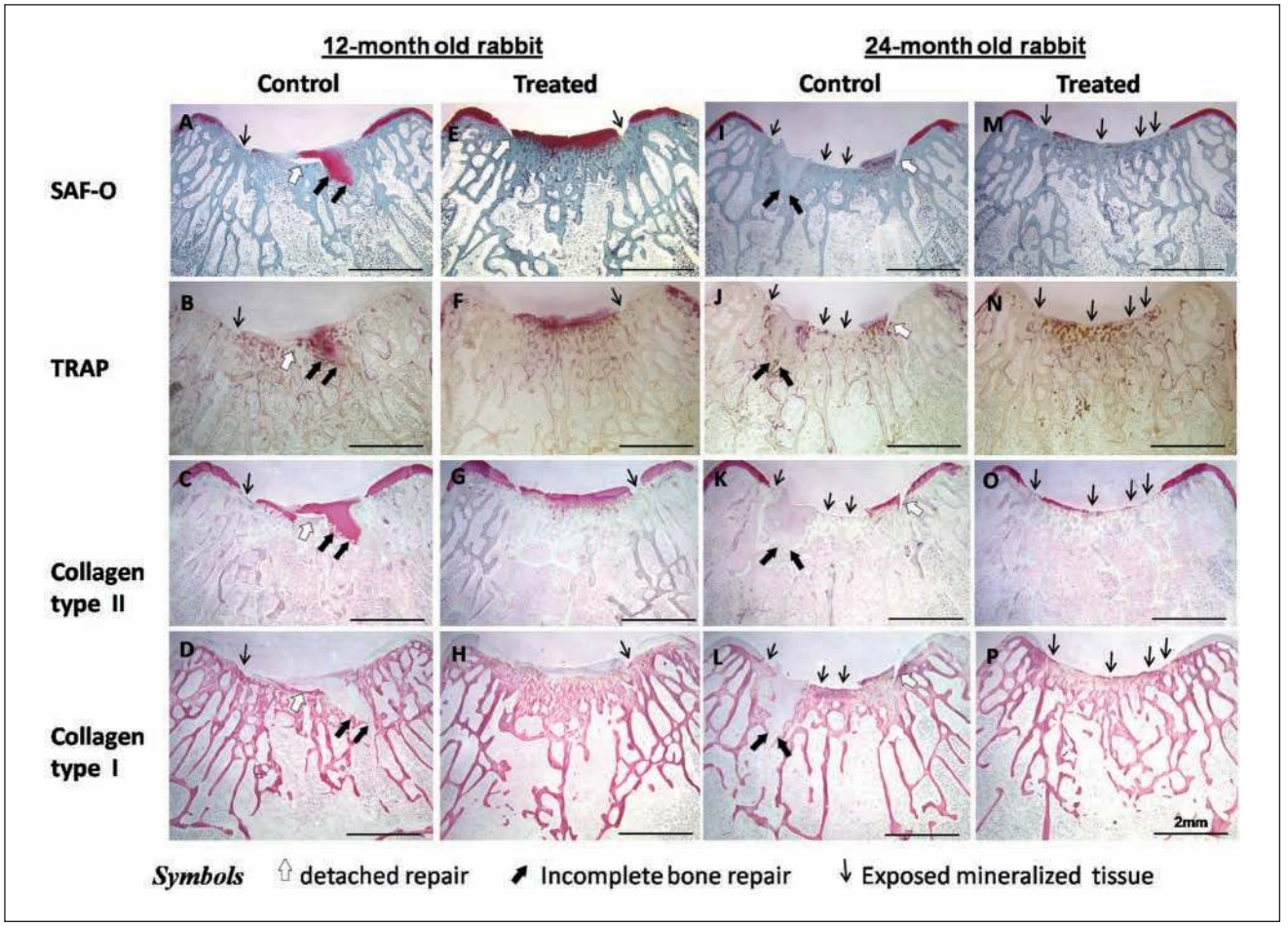

Figure 7. Histological appearance of bilateral 8-week repaired defects from the same 12-month-old (**A-H**) or 24-month-old (**I-P**) rabbit in adjacent sections collected through the middle of the drill holes stained for Safranin O, enzymatically stained for TRAP, and immunostained for collagen type I or collagen type II. In 10- to 12-month-old rabbits, a more integrated and hyaline repair cartilage tissue was obtained in defects treated with thrombin-chitosan-GP/blood implant compared to contralateral defects treated with thrombin only. Osteoclasts were detected in areas below endochondral repair (TRAP) (**E-H**). The 24-month-old rabbits showed a weaker cartilage repair response than 12-month-old rabbits.

Chitosan-GP/blood implants could also promote osteoclast formation through angiogenic activity after 2 weeks of repair. We recently showed that chitosan can attract angiogenic, arginase-1+ alternatively activated (AA) macrophages to subchondral bone and promote the formation of CD-31/PE-CAM+ angiogenic vessels at 2 weeks.[39] Angiogenesis could promote osteoclast formation by providing a local blood supply for monocyte extravasation. Blood vessels were detected in close vicinity of osteoclasts that formed on new woven bone and below endochondral repair (**Fig. 3 I** and **J**). It was recently reported that osteoclasts promote angiogenesis below the growth plate by releasing MMP-9, which is needed to untether VEGF from calcified cartilage matrix.[41] Others have generated *in vitro* evidence that osteoclast-conditioned media contain chemotactic factors for bone marrow–derived mesenchymal stem cells.[42] These collective observations suggest a functional relationship between osteoclasts, new subchondral blood vessels, and osteochondral regeneration.

Role of Chitosan Scaffold and Osteoclasts in Promoting Cartilage Repair and Integration

Treated repair tissues showed improved histological cartilage repair features compared to controls, which were similar to those previously obtained in the same rabbit model using nonfluorescent chitosan-GP/blood implants without thrombin,[9] including a well-integrated repair with approximately 85% collagen type II+ matrix, high cellularity, and chondrocyte-like phenotype. However, in this study, the total histology scores were lower, most probably due to the use of older rabbits (10-24 months) compared to the previous study (9-13 months).[9] This study also employed male and female rabbits compared to all female rabbits in

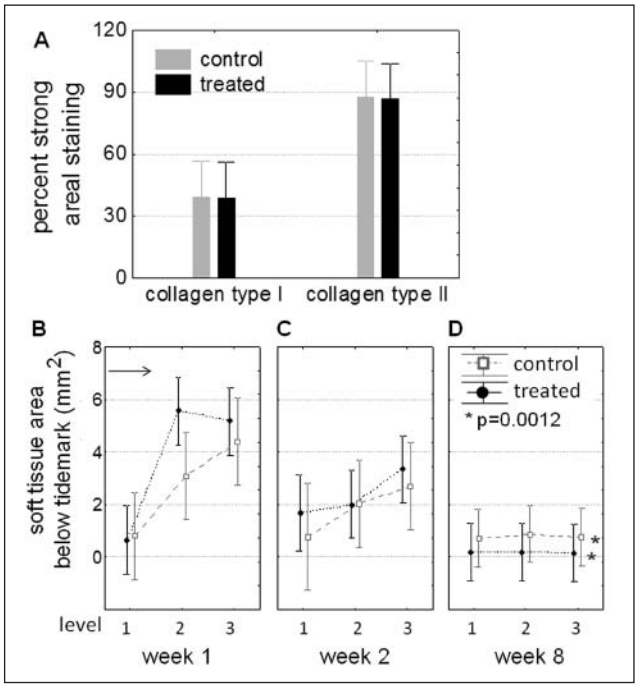

Figure 8. Quantitative measures of cartilage repair tissue collagen content and residual soft tissue area in microdrilled defects. (**A**) In 8-week repair tissues above the projected tidemark, collagen matrix composition through the drill holes was unchanged by treatment ($N = 7$, average ± standard deviation). (**B-C**) Soft tissue below the projected tidemark diminished over time in all drill holes; however, significantly more soft tissue remained below control defects at 8 weeks (**D;** $N = 7$, average ± 95% confidence intervals). Levels 1, 2, and 3 refer to sections analyzed between, at the edge, and through the drill holes. The horizontal arrow (**B**) refers to the theoretical initial area occupied by two 1.0-mm-diameter, 3.5-mm-deep microdrill holes.

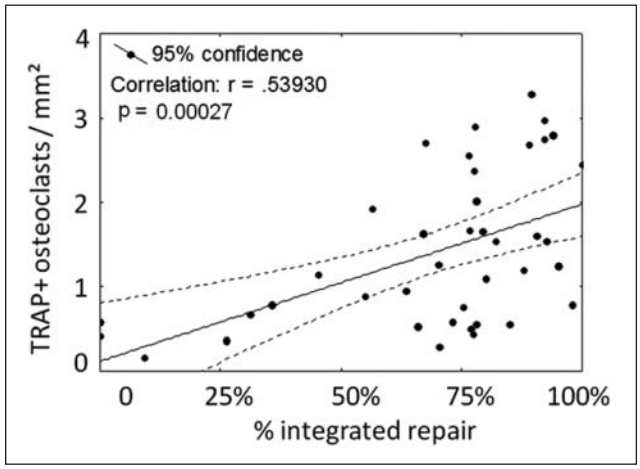

Figure 9. Subchondral TRAP+ osteoclast density at 8 weeks postoperatively correlated strongly with percentage of integrated repair (7 treated and 7 untreated defects, 3 sections per defect).

the former study. Older rabbits[43] and human patients over 40 years old[3,44] have an attenuated marrow-stimulation repair response that may be related to an age-dependent cell senescence leading to a decline in stem cells, chondrocyte mitotic potential, reduced aggrecan and collagen synthesis, reduced capacity to form glycosaminoglycan aggregates, and biomechanical weakening of the cartilage matrix.[45-49] In the present study, osteoclasts were detected in drilled subchondral bone of 24-month-old rabbits (**Fig. 7 J** and **N**), indicating that osteoclast recruitment alone is insufficient to stimulate hyaline repair in aged animals.

Our study sheds new light on how application of a scaffold-stabilized blood clot at surgery could guide a more integrated repair tissue well after the biomaterial has been cleared. Appositional growth of tissue from pre-existing bone needs to be initiated by a critical step of cell adhesion to bone, and the chitosan implant facilitates cell adhesion to bone in several distinct ways. Chitosan formed a cationic coating on the drill hole bone and the defect base (**Fig. 2A**), which could mediate cell adhesion to bone and to residual calcified cartilage surfaces that normally inhibit cartilage repair formation and integration.[9,21,50,51] Osteoclast-mediated access channels (**Fig. 3C**) could clear residual calcified cartilage and permit tissue anchored on bone to grow directly into the cartilage lesion. Osteoclasts lining the drill holes demineralize the bone surface and reveal collagen-binding sites for cell attachment.[52] By contrast, control drill hole repair cells tended to develop cohesive bonds with newly synthesized repair tissue matrix instead of bone (**Fig. 6 A** and **B**). This led to a detached and slightly hypertrophic repair tissue emanating from the drill hole, an observation consistent with the work of others.[7,53] Chitosan particle clearance was associated with diminished osteoclast recruitment to the side walls of treated drill holes and wound resolution.

Our model presents several limitations that should be noted. Human cartilage is much thicker than rabbit, with a different subchondral bone structure that could alter the timing and intensity of osteoclast recruitment and window of opportunity for cartilage-bone integration. In a cortical bone fracture model in skeletally mature sheep, osteoclast recruitment was delayed and peaked at 6 weeks after fracture.[18] These latter results were obtained in cortical and not trabecular bone fracture. Our study was also limited by the use of an acute trochlear defect model. Most clinical lesions are in the weightbearing condyle, and many are degenerative.[54] Nonetheless, given that humans and animals have common osteoclast activation pathways,[12-14,18,42] our data suggest that marrow stimulation in a clinical setting should elicit osteoclasts.

In conclusion, we have shown that subchondral drilling elicits osteoclasts through a 3-step process: resorption of damaged bone edges of the drill holes, remodeling of new woven bone, and recruitment below integrated endochondral repair cartilage. Enhanced acute recruitment of osteoclasts by chitosan implants was followed by improved repair integration and histological quality, which at 8

weeks postoperatively was a mixture of hyaline and fibrocartilage containing mostly collagen type II with some collagen type I. Altogether, these data suggest that osteoclasts play a role in promoting bone marrow–derived cartilage repair integration, which may improve durability of the resulting tissue.

Acknowledgments and Funding

Operating funds for this project were from the Canadian Institutes of Health Research (MOP 185810; principal investigator: C.D.H.) and the Canadian Arthritis Network. Salary support was provided by the Fonds de la Recherche en Santé du Quebec to C.D.H. (Bourse de Carrière Senior), C.M. (PhD fellowship), and V.L. (Groupe de Recherche en Sciences et Technologies Biomédicales). The authors thank G. Picard for excellent histology contributions.

Declaration of Conflicting Interests

J. S. is an employee of Piramal Healthcare (Canada). None of the other authors have any conflicts or apparent conflicts to declare.

References

1. Insall JN. Intra-articular surgery for degenerative arthritis of the knee: a report of the work of the late K. H. Pridie. J Bone Joint Surg Br. 1967;49(2):211-28.
2. Steadman JR, Rodkey WG, Singleton SB, Briggs KK. Microfracture technique for full-thickness chondral defects: technique and clinical results. Op Tech Orthop. 1997;7(4):300-4.
3. Knutsen G, Engebretsen L, Ludvigsen TC, Drogset JO, Grontvedt T, Solheim E, et al. Autologous chondrocyte implantation compared with microfracture in the knee: a randomized trial. J Bone Joint Surg Am. 2004;86A(3):455-64.
4. Saris DB, Vanlauwe J, Victor J, Haspl M, Bohnsack M, Fortems Y, et al. Characterized chondrocyte implantation results in better structural repair when treating symptomatic cartilage defects of the knee in a randomized controlled trial versus microfracture. Am J Sports Med. 2008;36(2):235-46.
5. Knutsen G, Drogset JO, Engebretsen L, Grontvedt T, Isaksen V, Ludvigsen TC, et al. A randomized trial comparing autologous chondrocyte implantation with microfracture. J Bone Joint Surg Am. 2007;89A(10):2105-12.
6. Nehrer S, Spector M, Minas T. Histologic analysis of tissue after failed cartilage repair procedures. Clin Orthop Relat Res. 1999;(365):149-62.
7. Mitchell N, Shepard N. The resurfacing of adult rabbit articular cartilage by multiple perforations through the subchondral bone. J Bone Joint Surg Am. 1976;58(2):230-3.
8. Breinan HA, Martin SD, Hsu HP, Spector M. Healing of canine articular cartilage defects treated with microfracture, a type-II collagen matrix, or cultured autologous chondrocytes. J Orthop Res. 2000;18(5):781-9.
9. Hoemann CD, Sun J, McKee MD, Chevrier A, Rossomacha E, Rivard GE, et al. Chitosan-glycerol phosphate/blood implants elicit hyaline cartilage repair integrated with porous subchondral bone in microdrilled rabbit defects. Osteoarthritis Cartilage. 2007;15(1):78-89.
10. Clark RA. Wound repair: overview and general considerations. In: Clark RA, editor. The molecular and cellular biology of wound repair. New York: Plenum Press; 1995. p. 3-35.
11. Davies JE. Bone engineering. In: Davies JE, editor. Toronto: Em Squared Inc.; 2000. p. 1-14.
12. Evans RA, Dunstan CR, Baylink DJ. Histochemical identification of osteoclasts in undecalcified sections of human bone. Miner Electrolyte Metab. 1979;2:179-85.
13. Boyce BF, Xing LP. Functions of RANKL/RANK/OPG in bone modeling and remodeling. Arch Biochem Biophys. 2008;473(2):139-46.
14. Simonet WS, Lacey DL, Dunstan CR, Kelley M, Chang MS, Luthy R, et al. Osteoprotegerin: a novel secreted protein involved in the regulation of bone density. Cell. 1997;89(2):309-19.
15. de Amorim F, Ornelas SS, Diniz SF, Batista AC, da Silva TA. Imbalance of RANK, RANKL and OPG expression during tibial fracture repair in diabetic rats. J Molec Histol. 2008;39(4):401-8.
16. Mosheimer BA, Kaneider NC, Feistritzer C, Sturn DH, Wiedermann CJ. Expression and function of RANK in human monocyte chemotaxis. Arthritis Rheum. 2004;50(7):2309-16.
17. Breuil V, Schmid-Antomarchi H, Schmid-Alliana A, Rezzonico R, Euller-Ziegler L, Rossi B. The receptor activator of nuclear factor (NF)kappa B ligand (RANKL) is a new chemotactic factor for human monocytes. FASEB J. 2003;17(12):1751-3.
18. Schell H, Lienau J, Epari DR, Seebeck P, Exner C, Muchow S, et al. Osteoclastic activity begins early and increases over the course of bone healing. Bone. 2006;38(4):547-54.
19. Aguirre JI, Plotkin LI, Stewart SA, Weinstein RS, Parfitt AM, Manolagas SC, Bellido T. Osteocyte apoptosis is induced by weightlessness in mice and precedes osteoclast recruitment and bone loss. J Bone Miner Res. 2006;21(4):605-15.
20. Lascau-Coman V, Buschmann MD, Hoemann CD. Rapid EDTA microwave decalcification of rabbit osteochondral samples preserves enzyme activity and antigen epitopes. J Bone Miner Res. 2008;23:S408-S408.
21. Hoemann CD, Hurtig M, Rossomacha E, Sun J, Chevrier A, Shive MS, Buschmann MD. Chitosan-glycerol phosphate/blood implants improve hyaline cartilage repair in ovine microfracture defects. J Bone Joint Surg Am. 2005;87A(12):2671-86.
22. Shive MS, Hoemann CD, Restrepo A, Hurtig MB, Duval N, Ranger P, et al. BST-CarGel: in situ chondroinduction for cartilage repair. Op Tech Orthop. 2006;16(4):271-8.
23. Buschmann MD, Hoemann CD, Hurtig MB, Shive MS. Cartilage repair with chitosan/glycerol-phosphate stabilised blood clots. In: Williams RJ, editor. Cartilage repair: analysis and strategies. Totowa, NJ: Humana Press; 2006. p. 83-106.
24. Chevrier A, Hoemann CD, Sun J, Buschmann MD. Chitosan-glycerol phosphate/blood implants increase cell recruitment, transient vascularization and subchondral bone remodeling in drilled cartilage defects. Osteoarthritis Cartilage. 2007;15(3):316-27.

25. Peluso G, Petillo O, Ranieri M, Santin M, Ambrosio L, Calabro D, et al. Chitosan-mediated stimulation of macrophage function. Biomaterials. 1994;15(15):1215-20.
26. Simard P, Galarneau H, Marois S, Rusu D, Hoemann C, Poubelle P, et al. Neutrophils exhibit distinct phenotypes toward chitosans with different degrees of deacetylation: implications for cartilage repair. Arthritis Res Ther. 2009;11(3):R74.
27. Okamoto Y, Inoue A, Miyatake K, Ogihara K, Shigemasa Y, Minami S. Effects of chitin/chitosan and their oligomers/monomers on migrations of macrophages. Macromolec Biosci. 2003;3(10):587-90.
28. Ueno H, Nakamura F, Murakami M, Okumura M, Kadosawa T, Fujinag T. Evaluation effects of chitosan for the extracellular matrix production by fibroblasts and the growth factors production by macrophages. Biomaterials. 2001;22(15):2125-30.
29. Ma O, Lavertu M, Sun J, Nguyen S, Buschmann MD, Winnik FM, Hoemann CD. Precise derivatization of structurally distinct chitosans with rhodamine B isothiocyanate. Carbohydr Polym. 2008;72(4):616-24.
30. Marchand C, Rivard GE, Sun J, Hoemann CD. Solidification mechanisms of chitosan-glycerol phosphate/blood implant for articular cartilage repair. Osteoarthritis Cartilage. 2009;17(7):953-60.
31. Chevrier A, Rossomacha E, Buschmann MD, Hoemann CD. Optimization of histoprocessing methods to detect glycosaminoglycan, collagen type II, and collagen type I in decalcified rabbit osteochondral sections. J Histotechnol. 2005;28(3):165-75.
32. Luna L. Histopathologic methods and color atlas of special stains and tissue artifacts. Gaithersburg, MD: American Histolab Inc.; 1992.
33. Miao DS, Scutt A. Recruitment, augmentation and apoptosis of rat osteoclasts in 1,25-(OH)(2)D-3 response to short-term treatment with 1,25-dihydroxyvitamin D-3 in vivo. BMC Musculoskelet Disord. 2002;3:16.
34. O'Driscoll SW, Keeley FW, Salter RB. Durability of regenerated articular cartilage produced by free autogenous periosteal grafts in major full-thickness defects in joint surfaces under the influence of continuous passive motion: a follow-up report at one year. J Bone Joint Surg Am. 1988;70(4):595-606.
35. Herman S, Kronke G, Schett G. Molecular mechanisms of inflammatory bone damage: emerging targets for therapy. Trends Molec Med. 2008;14(6):245-53.
36. Miao DS, He B, Karaplis AC, Goltzman D. Parathyroid hormone is essential for normal fetal bone formation. J Clin Invest. 2002;109(9):1173-82.
37. Chen HM, Sun J, Hoemann CD, Lascau-Coman V, Wei OY, McKee MD, et al. Drilling and microfracture lead to different bone structure and necrosis during bone-marrow stimulation for dartilage repair. J Orthop Res. 2009;27(11):1432-8.
38. Usami Y, Okamoto Y, Minami S, Matsuhashi A, Kumazawa NH, Tanioka S, Shigemasa Y. Migration of canine neutrophils to chitin and chitosan. J Vet Med Sci. 1994;56(6):1215-6.
39. Hoemann CD, Chen GP, Marchand C, Sun J, Tran-Khanh N, Chevrier A, et al. Scaffold-guided subchondral bone repair: implication of neutrophils and alternatively activated arginase-1+ macrophages. Am J Sports Med. 2010 Jun 3 [Epub ahead of print].
40. Chakravarti A, Raquil MA, Tessier P, Poubelle PE. Surface RANKL of Toll-like receptor 4-stimulated human neutrophils activates osteoclastic bone resorption. Blood. 2009;114(8):1633-44.
41. Cackowski FC, Anderson JL, Patrene KD, Choksi RJ, Shapiro SD, Windle JJ, et al. Osteoclasts are important for bone angiogenesis. Blood. 2009;115(1):140-9.
42. Kreja L, Brenner RE, Tautzenberger A, Liedert A, Friemert B, Ehrnthaller C, et al. Non-resorbing osteoclasts induce migration and osteogenic differentiation of mesenchymal stem cells. J Cellular Biochem. 2010;109(2):347-55.
43. Wei XC, Messner K. Maturation-dependent durability of spontaneous cartilage repair in rabbit knee joint. J Biomed Mater Res. 1999;46(4):539-48.
44. Mithoefer K, Williams RJ 3rd, Warren RF, Potter HG, Spock CR, Jones EC, et al. The microfracture technique for the treatment of articular cartilage lesions in the knee: a prospective cohort study. J Bone Joint Surg Am. 2005;87(9):1911-20.
45. Martin JA, Buckwalter JA. The role of chondrocyte senescence in the pathogenesis of osteoarthritis and in limiting cartilage repair. J Bone Joint Surg Am. 2003;85A:106-10.
46. Bolton MC, Dudhia J, Bayliss MT. Age-related changes in the synthesis of link protein and aggrecan in human articular cartilage: implications for aggregate stability. Biochem J. 1999;337:77-82.
47. Tran-Khanh N, Hoemann CD, McKee MD, Henderson JE, Buschmann MD. Aged bovine chondrocytes display a diminished capacity to produce a collagen-rich, mechanically functional cartilage extracellular matrix. J Orthop Res. 2005;23(6):1354-62.
48. Tang LH, Buckwalter JA, Rosenberg LC. Effect of link protein concentration on articular cartilage proteoglycan aggregation. J Orthop Res. 1996;14(2):334-9.
49. Temple-Wong MM, Bae WC, Chen MQ, Bugbee WD, Amiel D, Coutts RD, et al. Biomechanical, structural, and biochemical indices of degenerative and osteoarthritic deterioration of adult human articular cartilage of the femoral condyle. Osteoarthritis Cartilage. 2009;17(11):1469-76.
50. Shamis LD, Bramlage LR, Gabel AA, Weisbrode S. Effect of subchondral drilling on repair of partial-thickness cartilage defects of third carpal bones in horses. Am J Vet Res. 1989;50(2):290-5.
51. Breinan HA, Minas T, Hsu HP, Nehrer S, Sledge CB, Spector M. Effect of cultured autologous chondrocytes on repair of chondral defects in a canine model. J Bone Joint Surg Am. 1997;79(10):1439-51.
52. Everts V, Delaisse JM, Korper W, Jansen DC, Tigchelaar-Gutter W, Saftig P, Beertsen W. The bone lining cell: its role in cleaning Howship's lacunae and initiating bone formation. J Bone Miner Res. 2002;17(1):77-90.
53. Pineda S, Pollack A, Stevenson S, Goldberg V, Caplan A. A semiquantitative scale for histologic grading of articular-cartilage repair. Acta Anat. 1992;143(4):335-40.
54. Robertson A, Chisholm T, Stanish WD. The use of biological materials in cartilage repair: current concepts. Techniques in Knee Surgery. 2008;7(3):191-202.